AD-A049 271 DAVID W TAYLOR NAVAL SHIP RESEARCH AND DEVELOPMENT CE--ETC F/G 20/4
A DISCRETE VORTEX SIMULATION OF A TWO-DIMENSIONAL SHEAR LAYER W--ETC(U)
DEC 77 W J GRABOWSKI, J G TELSTE

UNCLASSIFIED CMLD-77-26 NL

| OF |
AD
A049 271

END
DATE
FILMED
2-78
DDC

(12)

DAVID W. TAYLOR NAVAL SHIP RESEARCH AND DEVELOPMENT CENTER

Bethesda, Md. 20084

A DISCRETE VORTEX SIMULATION OF A TWO-DIMENSIONAL SHEAR LAYER WITH PREDICTION OF THE HYDRODYNAMIC NOISE

by

Walter J. Grabowski
and
John G. Telste

APPROVED FOR PUBLIC RELEASE: DISTRIBUTION UNLIMITED.

COMPUTATION, MATHEMATICS, AND LOGISTICS DEPARTMENT
DEPARTMENTAL REPORT

DECEMBER 1977

CMLD-77-26

MAJOR DTNSRDC ORGANIZATIONAL COMPONENTS

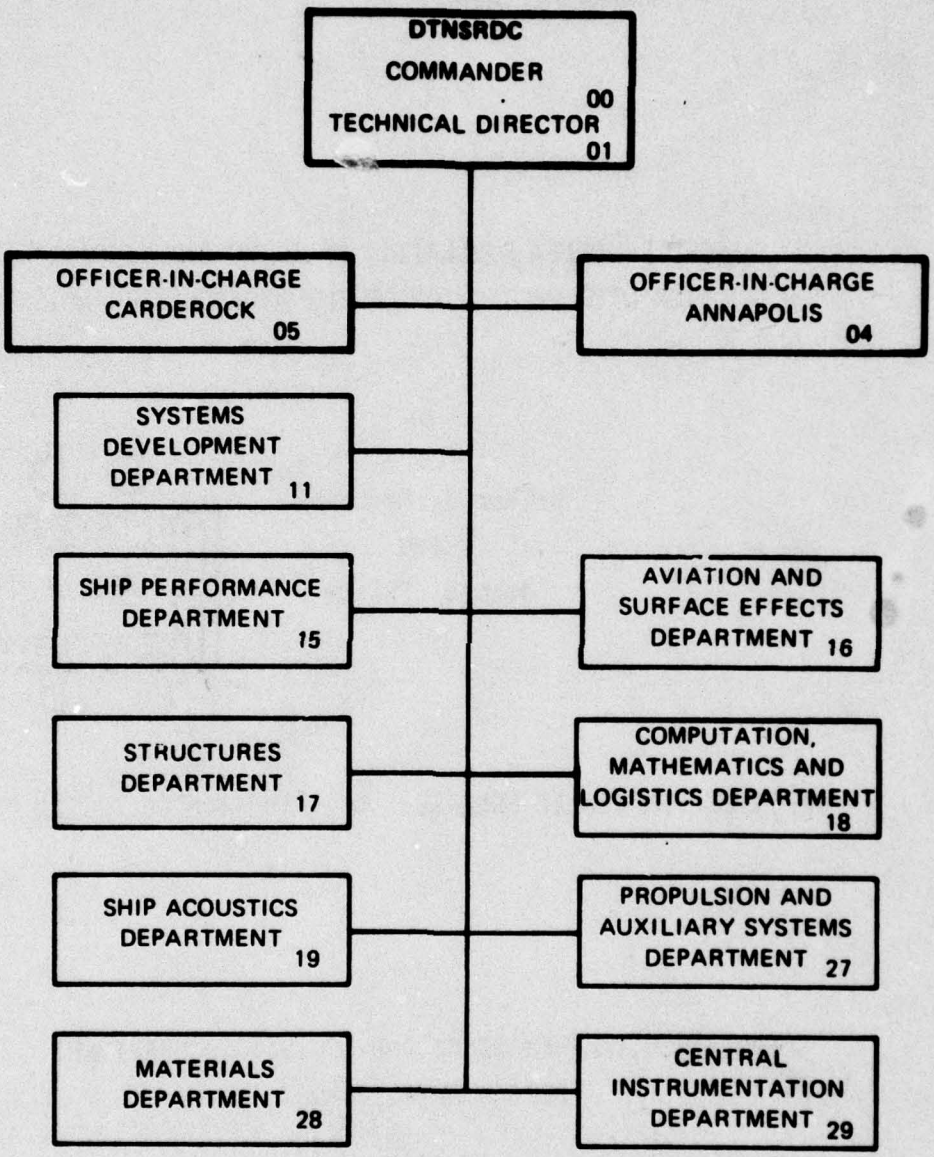

UNCLASSIFIED

SECURITY CLASSIFICATION OF THIS PAGE (When Data Entered)

REPORT DOCUMENTATION PAGE

READ INSTRUCTIONS BEFORE COMPLETING FORM

1. REPORT NUMBER: CMLD-77-26 ✓
2. GOVT ACCESSION NO.
3. RECIPIENT'S CATALOG NUMBER

4. TITLE (and Subtitle): A Discrete Vortex Simulation of a Two-Dimensional Shear Layer with Prediction of the Hydrodynamic Noise
5. TYPE OF REPORT & PERIOD COVERED
6. PERFORMING ORG. REPORT NUMBER

7. AUTHOR(s): Walter J. Grabowski, John G. Telste
8. CONTRACT OR GRANT NUMBER(s): ZR0140202

9. PERFORMING ORGANIZATION NAME AND ADDRESS: David W. Taylor Naval Ship R&D Center ✓, Bethesda, Maryland 20084
10. PROGRAM ELEMENT, PROJECT, TASK AREA & WORK UNIT NUMBERS: 61152N, ZR0140201, 1-1843-020

11. CONTROLLING OFFICE NAME AND ADDRESS
12. REPORT DATE: December 1977
13. NUMBER OF PAGES: 35

14. MONITORING AGENCY NAME & ADDRESS (if different from Controlling Office): 34p.
15. SECURITY CLASS. (of this report): UNCLASSIFIED
15a. DECLASSIFICATION/DOWNGRADING SCHEDULE

16. DISTRIBUTION STATEMENT (of this Report)

APPROVED FOR PUBLIC RELEASE: DISTRIBUTION UNLIMITED.

17. DISTRIBUTION STATEMENT (of the abstract entered in Block 20, if different from Report)

18. SUPPLEMENTARY NOTES

19. KEY WORDS (Continue on reverse side if necessary and identify by block number)

Hydrodynamic Noise
Vortex Sound
Computational Fluid Dynamics

20. ABSTRACT (Continue on reverse side if necessary and identify by block number)

A numerical simulation of the two-dimensional shear layer occurring at the interface of two streams of different velocity is described. The shear layer is represented by a large number of discrete vortices and is allowed to evolve in accordance with the velocity potential of the vortices. It is found that the model effectively simulates the large-scale evolution of the layer. The model, however, is found to be inadequate for predicting the hydrodynamic sound generated in the shear layer because small-scale vortex motion plays a major role in acoustic prediction.

DD FORM 1 JAN 73 1473 EDITION OF 1 NOV 65 IS OBSOLETE
S/N 0102-014-6601

UNCLASSIFIED

SECURITY CLASSIFICATION OF THIS PAGE (When Data Entered)

406 847

4B

TABLE OF CONTENTS

LIST OF FIGURES

LIST OF FIGURES (cont.)

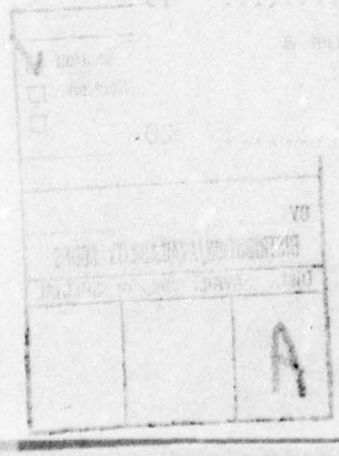

ABSTRACT

A numerical simulation of the two-dimensional shear layer occuring at the interface of two streams of different velocity is described. The shear layer is represented by a large number of discrete vortices and is allowed to evolve in accordance with the velocity potential of the vortices. It is found that the model effectively simulates the large-scale evolution of the layer. The model, however, is found to be inadequate for predicting the hydrodynamic sound generated in the shear layer because small-scale vortex motion plays a major role in acoustic prediction.

1. INTRODUCTION

1.1 BACKGROUND

The two-dimensional mixing layer generated at the interface of two streams having different velocity and not necessarily having the same physical properties has recently been the subject of much theoretical and experimental study.[1] This layer is an archetype of all shear flows because it demonstrates in simple fashion the processes of turbulent energy production, mixing, and entrainment which are fundamental to such flows. Much of the research to date has been devoted to examination of the "large coherent structure" of the turbulence within the layer. It appears that the large scale turbulent motion within the layer, and in other turbulent shear flows, is in some sense deterministic. The individual events associated with this large scale motion (for example, eddy growth and interaction) occur in a particular sequence and reoccur randomly, but with a statistically definable mean period. Of course the importance of large

[1] References are given on page 28.

turbulent eddies was postulated by Townsend[2] over twenty years ago, but these eddies were viewed as entirely random, short-lived phenomena. However, the visual and quantitative observations of the development of spatially coherent patterns within the turbulent mixing layer by Brown and Roshko[3] and by Winant and Browand,[4] and within a turbulent boundary layer by the Stanford University group,[5,6,7] have brought about a redirection of much research into the turbulence problem and a revision of many long accepted views as to its nature. The current view is that the large scale motion, in particular the interaction between the coherent structures, dominates the evolution and growth of the shear layer. Similar importance has been attached to large structures observed in boundary-layer flows and in the near-nozzle mixing region of axisymmetric jets.[8,9,10]

The new awareness of the significance of large scale coherent structures in turbulent flows has led several researchers to suggest that these structures might play a role in the not well understood mechanisms responsible for the hydrodynamic sound generated in shear flows.[11] If this supposition is correct and if such structures are in some sense deterministic, then major advances in the prediction of hydrodynamic sound might be within reach.

The significance and role of large structures in sound generation, is, however, a subject of much controversy. For example, the experiments of Crow and Champagne,[8] Moore,[9] and Lau and Fisher[10] have amply demonstrated that large structures are a major if not dominant flow constituent in the first four to six diameters downstream of the exit of an axisymmetric jet, and it is a widely held belief that at least half of the total sound power emitted by such jets originates from sources within the first four diameters. A connection between the coherent structures and at least part of the acoustic output might thus be expected. Crow's experiments,[11] in fact, suggest a close relationship. Crow performed far-field acoustic experiments in which a jet was excited internally over a range of Strouhal numbers ($St = fD/U_e$ where f is the excitation frequency, D is the nozzle diameter, and U_e is the exit velocity). He measured a peak gain of as much as 30 dB (or a factor of about 2500) in the far-field noise filtered about a Strouhal number of 0.3. This Strouhal number corresponded to a

preferred frequency for the growth of disturbances in the jet mixing layer and for the generation of eddy-like large structures. Crow found no change in the broad-band noise in response to this forcing. In a more recent but quite similar study, however, Moore[9] found that even with excitation at a preferred frequency for disturbance growth (St $\approx$ 0.5 in his experiment) there was no significant increase in the far-field noise filtered about this frequency. There was, moreover, an increase of 5-8 dB in broadband noise. The results of Crow and Moore are strongly at variance and, as Crighton notes,[12] even the fact that Crow's exit velocities were slightly supersonic and Moore's subsonic does not explain the differences. Crow's results suggest that the large eddy behavior is directly responsible for significant acoustic output, whereas Moore has suggested that the sound is generated by smaller scale turbulent motion which may be modified through a highly non-linear process by the excitation of large scale eddies.

Although the experimental results of Crow and Moore differ substantially, both indicate that large coherent structures play a significant noise-producing role. There have been several attempts to numerically predict the hydrodynamic sound generated in shear flows. In all of these the assumption that large scale structure plays a dominant role was implicit. Davies et al[13] attempted to develop a model based on a discrete vortex representation of the mixing layer for the calculation of the noise from an axisymmetric jet. Although a peak in the computed noise spectrum was found at about St = 0.5, most of the characteristics of jet noise were not well represented. Hardin and Mason[14] developed a discrete vortex model for noise generated by shear flow over the mouth of a cavity. While they include in their paper no direct comparison with experiment, they do claim that the model explains certain frequency and directivity phenomena. Neither Davies et al nor Hardin and Mason included mean-flow refraction or "shrouding" effects. In unpublished work (1975), Lugt et al attempted to calculate the noise generated in a two-dimensional mixing layer represented by discrete vortices. Using no more than 48 discrete vortices, they found that they could not adequately represent the mixing layer and hence that the calculated sound power had no physical meaning. Both Hardin and Mason and Lugt et al based their models for noise generation on Powell's[15]

formulation of the acoustic source terms. Using a more direct approach, Metcalfe and Orszag[16] attempted to model jet fluctuations with solutions of the complete three-dimensional Navier-Stokes equations. According to Metcalfe[17] this effort was not successful due mostly to an inability to obtain sufficient statistical properties from the flow simulation.

This report presents the results of an effort to develop a mathematical/numerical model for the acoustic radiation of a simple two-dimensional mixing layer subject to an applied disturbance. It examines discrete vortex-type approximations for the prediction of hydrodynamic sound and hopefully provides some insight into their utility.

1.2 MIXING LAYER SIMULATION - LARGE COHERENT STRUCTURES

Several recent attempts to model the behavior of the mixing layer have emphasized the characteristics of the large scale structure. Winant and Browand[4] proposed a very simple model which consists of two vertically offset infinite arrays of equispaced line vortices. According to the authors the vortices were found to rotate about one another and "draw closer together" (presumably in the mean-flow direction) while the distance between the vortex rows increased. Qualitative agreement between predictions of the model and experiment was asserted for the layer growth rate.

Acton,[18] however, argued that a model for the evolution of the mixing layer, especially for the coalescense of large vortical structures, requires consideration of finer details of the layer structure. Acton therefore modeled the mixing layer with a distribution of discrete vortices such that a single coherent structure consisted of an amalgam of many discrete vortices. He considered a spatially periodic disturbance of an infinite discretized shear layer such that each period consisted of two sinusoidal "waves" displaced vertically relative to each other. Initially, vortices in each of the "waves" roll up into rotating concentrations which subsequently revolve about each other until they coalesce (see Figure 2 of this report for the results of a similar simulation). The behavior reported by Acton is in good qualitative agreement with the "pairing" description of Winant and Browand.

Most recently, Ashurst[19] reported a numerical simulation of the mixing layer using the discrete vortex approach without the assumption of periodicity. He was able to obtain good agreement with the experimental data of Browand and Weidman[20] for the mixing layer growth and the time-averaged Reynolds stress profile within the layer. These calculations used several thousand discrete vortices, were quite expensive, and yielded a very fine color film of the shear-layer evolution.

The research reported here extends the basic approach of Acton, incorporates additional vortices, and attempts to compute from the vortex motion the hydrodynamic sound generated by the shear-layer. The assumption of periodicity is not overly restrictive for the purpose of this study, and it allows the major aspects of shear layer behavior to be simulated economically.

2. DISCRETE VORTEX SHEAR-LAYER SIMULATION

We consider a two-dimensional shear layer which extends infinitely far in the positive and negative x_1-directions (Figure 1). The flow velocity far above the layer is -U and the velocity below is U. The shear layer of thickness δ_0 at time t_0 represents the lateral region (in x_2) over which the velocity varies from -U to U. The velocity components in the x_1- and x_2-directions are denoted by u_1 and u_2, respectively. In order to investigate the nonlinear evolution of the shear layer which results from the imposition of a spatial disturbance, we represent the vorticity $\omega = \partial u_2/\partial x_1 - \partial u_1/\partial x_2$, within the layer, by a distribution of discrete point vortices each with circulation Γ. We distribute the vortices in cyclic fashion over longitudinal sections of length λ with N vortices per section, and we consider the motion of the vortices within one cycle and assume that the motion in all other cycles is identical. The motion is thus periodic with period λ. We assume that the effects of viscosity are important only at very small scales of motion so that they may be safely ignored.

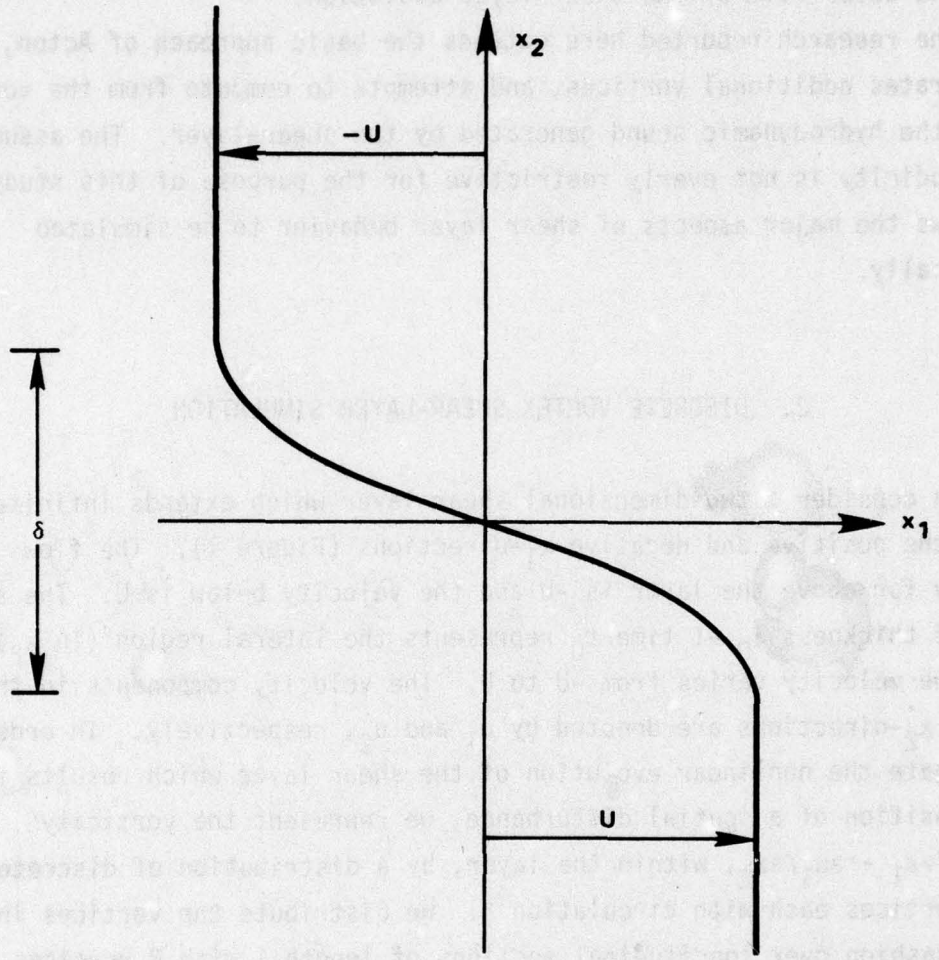

Figure 1. Shear-Layer Geometry

2.1 EQUATIONS OF MOTION

The complex potential $w = u_1 + iu_2$ of a single infinite row of equidistant vortices of strength Γ and spacing λ is

$$w(z) = \frac{i\Gamma}{2\pi} \ln \sin\left(\frac{\pi z}{\lambda}\right)$$

where $z = x_1 + i\,x_2$. Separating the real and imaginary components of w, we obtain

$$u_1(x_1,x_2) = -\frac{\Gamma}{2\lambda} \frac{\sinh 2\pi\, x_2/\lambda}{\cosh 2\pi\, x_2/\lambda - \cos 2\pi\, x_1/\lambda}$$

and

$$u_2(x_1,x_2) = \frac{\Gamma}{2\lambda} \frac{\sin 2\pi\, x_1/\lambda}{\cosh 2\pi\, x_2/\lambda - \cos 2\pi\, x_1/\lambda}$$

Each of the N vortices distributed within a cycle may be viewed as a member of a different infinite row so that we represent the layer by N rows of equidistant vortices. Then the velocity at any point induced by all N rows of vortices is given by

$$u_1(x_1,x_2) = \sum_{j=1}^{N} \left(-\frac{\Gamma}{2\lambda}\right) \frac{\sinh 2\pi(x_2-x_{2,j})/\lambda}{\cosh 2\pi(x_2-x_{2,j})/\lambda - \cos 2\pi(x_1-x_{1,j})/\lambda} \qquad (1)$$

and

$$u_2(x_1,x_2) = \sum_{j=1}^{N} \left(\frac{\Gamma}{2\lambda}\right) \frac{\sin 2\pi(x_1-x_{1,j})/\lambda}{\cosh 2\pi(x_2-x_{2,j})/\lambda - \cos 2\pi(x_1-x_{1,j})/\lambda} \qquad (2)$$

where $(x_{1,j}, x_{2,j})$ is the position of the j^{th} vortex within the cycle. Note that as x_2 approaches $\pm\infty$, u_1 approaches $\mp U = \Gamma N/2\lambda$ so that the required vortex strength Γ is $2\lambda U/N$.

In inviscid incompressible flow vorticity convects with fluid elements so that Equations (1) and (2) can be used to describe the motion of each vortex, i.e.,

$$\frac{dx_{1,j}}{dt} = u_1(x_{1,j},x_{2,j}) \equiv u_{1,j} \qquad (3)$$

and

$$\frac{dx_{2,j}}{dt} = u_2(x_{1,j},x_{2,j}) \equiv u_{2,j} \tag{4}$$

Equations (3) and (4) determine the motion of the j^{th} vortex in terms of the N-1 other vortices in the cycle. The velocities $u_{1,j}$ and $u_{2,j}$ are given by Equations (1) and (2). For purposes of computation, we non-dimensionalize as follows:

$$u_1^* = 2\lambda u_1/\Gamma N$$

$$u_2^* = 2\lambda u_2/\Gamma N$$

$$x_1^* = x_1/\lambda$$

$$x_2^* = x_2/\lambda$$

and

$$t^* = t\Gamma N/2\lambda^2$$

Then

$$\frac{dx_{1,i}^*}{dt^*} = u_{1,i}^* = -\frac{1}{N}\sum_{\substack{j=1\\ j\neq i}}^{N} \frac{\sinh 2\pi(x_{2,i}^*-x_{2,j}^*)}{\cosh 2\pi(x_{2,i}^*-x_{2,j}^*)-\cos 2\pi(x_{1,i}^*-x_{1,j}^*)} \tag{5}$$

and

$$\frac{dx_{2,i}^*}{dt^*} = u_{2,i}^* = \frac{1}{N}\sum_{\substack{j=1\\ j\neq i}}^{N} \frac{\sin 2\pi(x_{1,i}^*-x_{1,j}^*)}{\cosh 2\pi(x_{2,i}^*-x_{2,j}^*)-\cos 2\pi(x_{1,i}^*-x_{1,j}^*)} \tag{6}$$

and u_1^* approaches ± 1 as x_2^* approaches $\mp\infty$.

Equations (5) and (6) constitute a system of 2N coupled, non-linear, ordinary differential equations. With suitable initial conditions (the x_1, x_2 position of each vortex) these equations determine the subsequent motion of the vortices and the evolution of the layer. In this study the equations were solved numerically using, during the early stages, a fourth-order Runge-Kutta method; solutions from which acoustic radiation were calculated were obtained with a sixth-order Milne predictor-corrector algorithm since it was found that much greater accuracy was required.

All the calculations described in this report were performed on the

Texas Instruments Advanced Scientific Computer at the Naval Research Laboratory with double precision arithmetic. DTNSRDC users access this computer from a remote job entry terminal at DTNSRDC. Certain data were transferred via punched cards and magnetic tape to the CDC 6700 at DTNSRDC where the TIMAGE interactive graphics system and the DISSPLA computer graphics package were used to generate most of the figures.

2.2 SHEAR-LAYER EVOLUTION

Figures 2a through 2h show a sample simulation of the evolution of a shear layer represented by 256 vortices per period λ. The shear layer of initial thickness 0.05 is assumed to have been disturbed by some external means and at t=0 has the configuration shown in Figure 2a. Note that each wavelength consists of two sinusoidal "waves", each of length 1/2, which are displaced vertically relative to each other a distance 0.02. Each of the waves has amplitude -0.05. Vortices in the left-hand and right-hand "waves" are marked with O's and X's, respectively. The integration was performed with the Runge-Kutta method with time step 0.005 and required 101 CP seconds to reach t*=1.0. During the initial stages of the evolution (Figures 2a-2d), the vorticity in both "waves" concentrates in nearly identical fashion. (The behavior would be identical were it not for the vertical displacement.) As the shear layer continues to evolve, the two vortex amalgams interact, rotate about each other (Figures 2e-2g), and coalesce (Figure 2h). This process is quite similar to the "pairing" process observed experimentally by Winant and Browand.[4] The elongation of the structures in the flow (x_1) direction (see especially Figure 2e) was also observed experimentally by Winant and Browand who described the vortices as taking on a "more or less elliptic shape with major-to-minor axis ratio of 2." It is also clear that fluid is transported to the opposite side of the mixing layer before being ingested into the central region. Again similar behavior was noted by Winant and Browand.

On the basis of this simulation and other simulations we have performed, we believe that discrete vortex simulation can effectively model the large scale behavior of the shear layer. Acton,[18] who used only 96 vortices, performed extensive calculations with his model and has presented

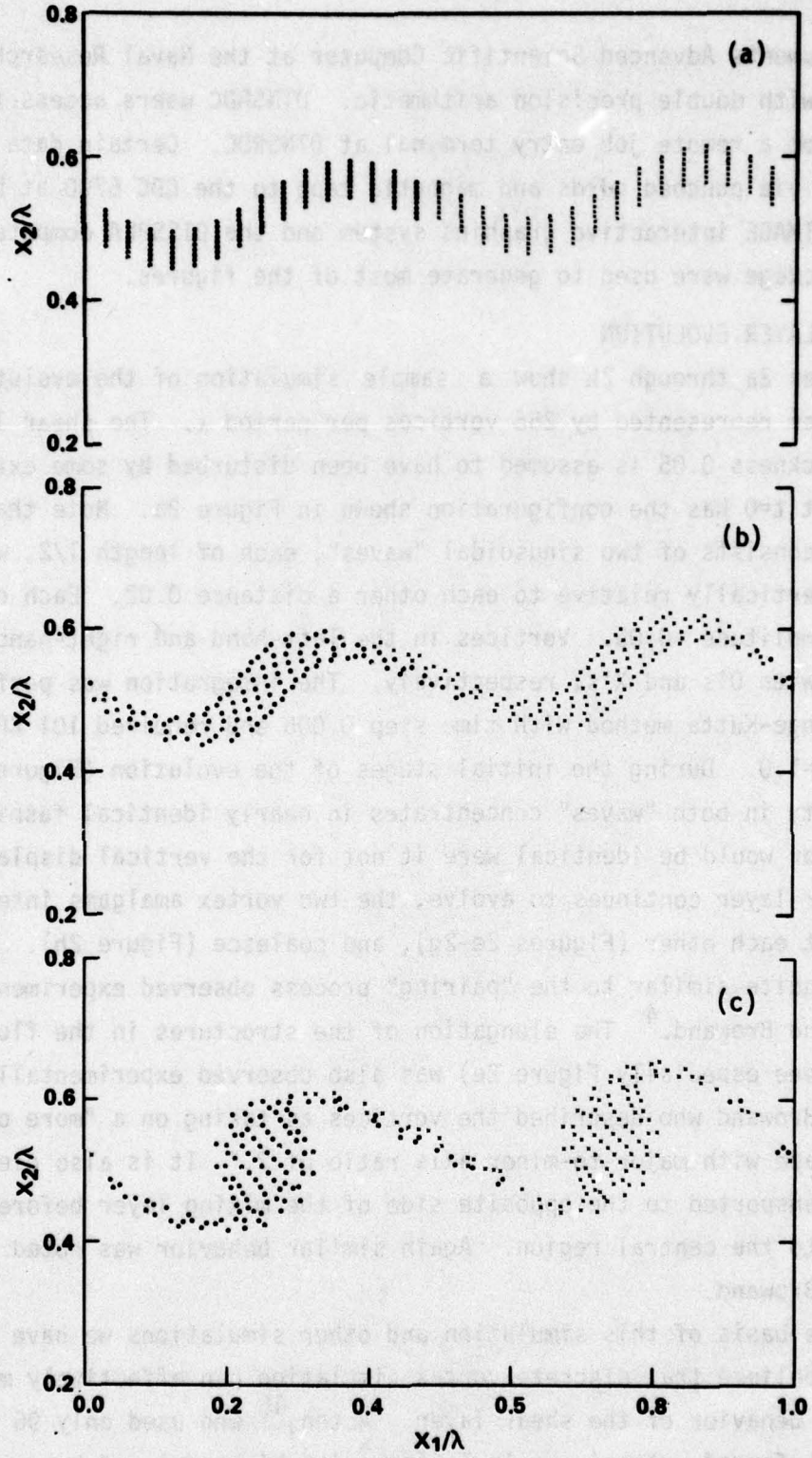

Figures 2 (a-c). For legend see page 12.

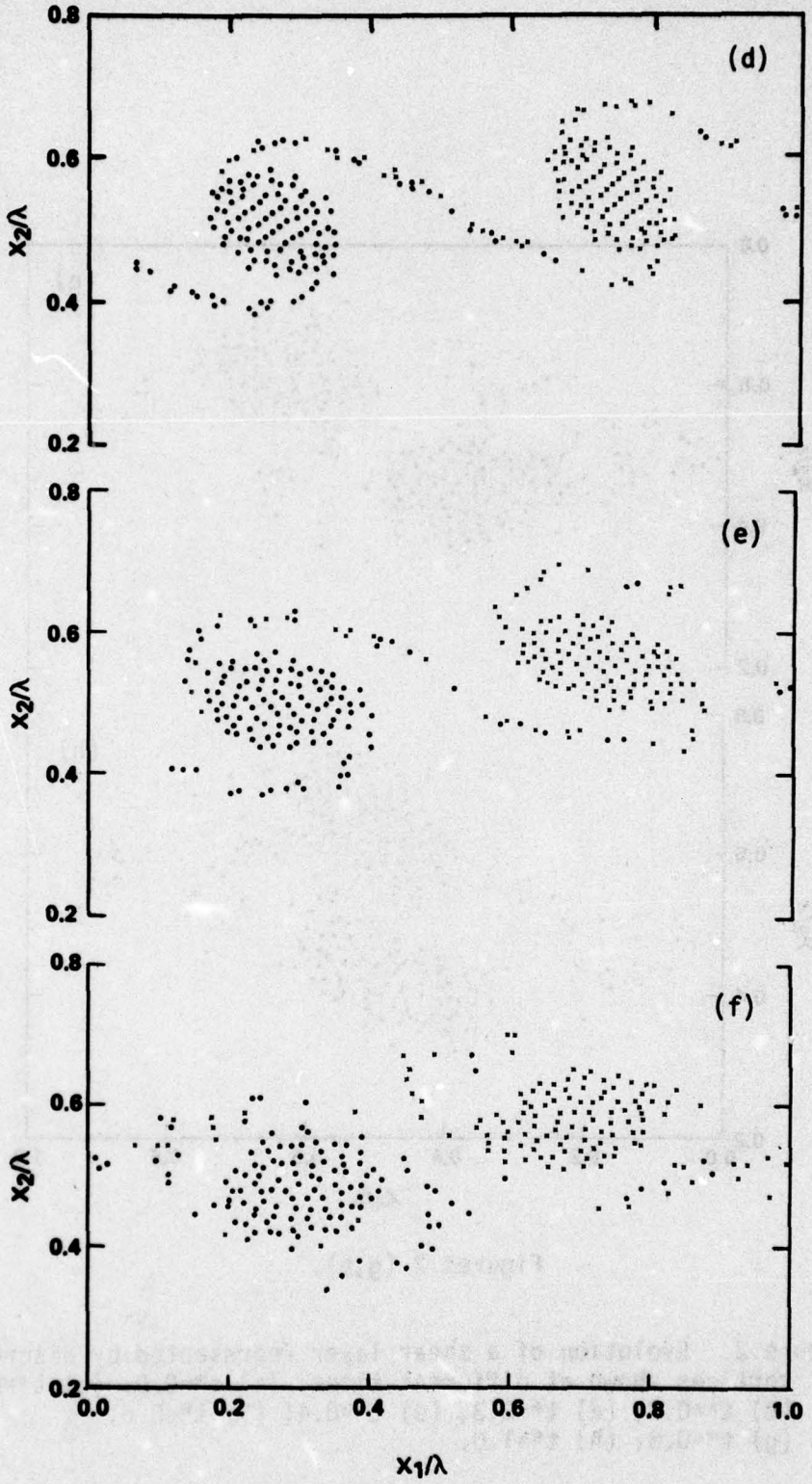

Figures 2 (d-f). For legend see next page.

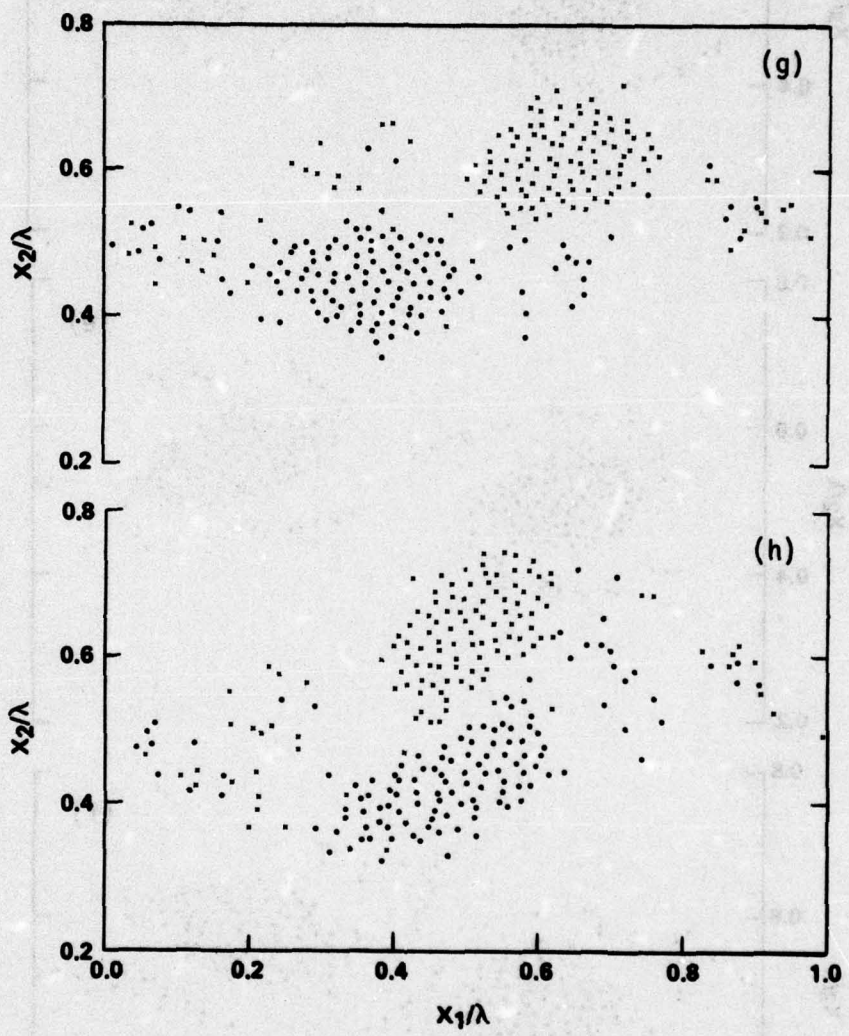

Figures 2 (g,h).

Figure 2. Evolution of a shear layer represented by discrete vortices shown at different times: (a) t*=0.0; (b) t*=0.1; (c) t*=0.2; (d) t*=0.3; (e) t*=0.4; (f) t*=0.6; (g) t*=0.8; (h) t*=1.0.

his results in great detail, including comparisons with experimental data. The overall characteristics of the shear-layer evolution shown in Figures 10a through 10h in his paper are in excellent agreement with the calculation presented above. His paper is recommended to the interested reader.

3. VORTICITY-GENERATED HYDRODYNAMIC SOUND

3.1 MATHEMATICAL FORMULATION

To develop an estimate for the acoustic radiation from the evolving shear layer we begin with Lighthill's[21] fundamental expression for the acoustic radiation generated by a compact region of fluctuating flow in an otherwise quiescent fluid:

$$\frac{\partial^2 \rho}{\partial t^2} - c_0^2 \frac{\partial^2 \rho}{\partial x_i^2} = \frac{\partial^2 T_{ij}}{\partial x_i \partial x_j} \tag{7}$$

where $T_{ij} = \rho_0 u_i u_j$, c_0 and ρ_0 are the ambient undisturbed sound speed and density, and u_i is the fluid velocity computed with the assumption of incompressibility. In applying Equation (7) to the shear layer we assume that $U/c_0 << 1$. Powell[15] attempted to identify the source of sound with the fluctuating vorticity field and he suggested that the right-hand forcing term in Equation (7) should be replaced by $\rho_0 \nabla\cdot(\vec{\omega} \times \vec{v})$ where $\vec{\omega}$ and $\vec{v}$ are the local vorticity and velocity. Powell's assumption was verified in rigorous fashion by Howe[22] who showed that

$$\frac{\partial^2 T_{ij}}{\partial x_i \partial x_j} \approx \rho_0 \nabla\cdot(\vec{\omega} \times \vec{v}) \tag{8}$$

for small turbulence Mach numbers. Thus, specification of $\vec{\zeta} = \vec{\omega} \times \vec{v}$ over the fluctuating region (which is assumed to be small--its characteristic dimension is much smaller than an acoustic wavelength) yields an estimate for the acoustic radiation.

The formal solution to Equation (7) with the source term of Expression (8) is obtained using a Green's function and is

$$\frac{\rho(\vec{x},t)-\rho_0}{\rho_0} = \frac{1}{4\pi c_0^2} \int_\tau \int_{\vec{y}} (\nabla_y \cdot \vec{\zeta}) \frac{\delta(t-\tau-|\vec{x}-\vec{y}|/c_0)}{|\vec{x}-\vec{y}|} d^3\vec{y}\, d\tau$$

This kind of solution is sometimes termed a retarded potential. The acoustic signal reaching $\vec{x}$ at time t originates at position $\vec{y}$ within the fluctuating region at $t-|\vec{x}-\vec{y}|/c_0$. We apply the usual simplifications to this integral (for example, see Lighthill[21] and Crighton[12]). We make use of the properties of linear differential operators applied to convolution products and then perform the τ-integration to obtain

$$\frac{\rho(\vec{x},t)-\rho_0}{\rho_0} = \frac{1}{4\pi c_0^2} \nabla_x \cdot \int_{\vec{y}} \vec{\zeta}(\vec{y},t-|\vec{x}-\vec{y}|/c_0) \frac{d^3\vec{y}}{|\vec{x}-\vec{y}|}$$

We then perform the x-differentiation and ignore a higher-order term so that

$$\frac{\rho(\vec{x},t)-\rho_0}{\rho_0} = -\frac{1}{4\pi c_0^2} \int_{\vec{y}} \left(\frac{\vec{x}-\vec{y}}{c_0|\vec{x}-\vec{y}|^2}\right) \cdot \frac{\partial \vec{\zeta}}{\partial t}(\vec{y},t-|\vec{x}-\vec{y}|/c_0) d^3\vec{y}$$

Finally, we assume that the eddy region is compact, that is, its characteristic linear dimension is much smaller than the acoustic wavelengths of the sound it generates, and that $\vec{x}-\vec{y} \approx \vec{x}$, so that we consider only the far-field acoustic radiation. We obtain

$$\frac{\rho(\vec{x},t)-\rho_0}{\rho_0} = \frac{1}{4\pi c_0^4 |\vec{x}|} \frac{\partial^2}{\partial t^2} \int_{\vec{y}} \left(\frac{\vec{x}\cdot\vec{y}}{|\vec{x}|}\right) \frac{\vec{x}}{|\vec{x}|} \cdot \vec{\zeta}(\vec{y},t-|\vec{x}|/c_0) d^3\vec{y} \qquad (9)$$

Equation (9) shows that, to first order, the acoustic radiation is determined from the second time derivative of $\vec{\zeta}$. Note that the acoustic signal at $\vec{x}$ at time t is now related, through the second time derivative, to fluctuations at the same time, $t-|\vec{x}|/c_0$, for all locations $\vec{y}$.

We may evaluate $\vec{\zeta}$ and its time derivatives in a simple fashion for an array of discrete point vortices. For such an array

$$\vec{\omega}(\vec{y},t) = \sum_{j=1}^{N} \vec{\omega}_j = \sum_{j=1}^{N} \Gamma\, \delta(x_{1,j}-y_1)\delta(x_{2,j}-y_2)\hat{e}_3 \qquad (10)$$

where $\hat{e}_3$ is a unit vector normal to the plane of motion. We substitute Equation (10) into Equation (9) and perform the $\vec{y}$ integration (which is made easy by the appearance of δ functions) to yield the acoustic radiation per unit length (in the $\hat{e}_3$-direction) at $\vec{x}=x_1\hat{e}_1+x_2\hat{e}_2+x_3\hat{e}_3$

$$\frac{\rho(\vec{x},t)-\rho_0}{\rho_0 \Delta y_3} = \frac{1}{4\pi c_0^4 |\vec{x}|} \frac{d^2}{dt^2} \sum_{j=1}^{N} \left(\frac{\vec{x}\cdot\vec{x}_j}{|\vec{x}|} \right) \frac{\vec{x}}{|\vec{x}|} \cdot (\Gamma \hat{e}_3 \times \vec{u}_j) \qquad (11)$$

where $\vec{u}_j = \dot{\vec{x}}_j$, the velocity of the j^{th} vector, and $\vec{u}_j$ and $\vec{x}_j$ are evaluated at $t-|\vec{x}|/c_0$. This acoustic radiation is due to flow fluctuations in the plane x_3 = constant. Equation (11) is written in terms of the previously defined non-dimensional variables as

$$\frac{\rho(\vec{x}^*, t^*)-\rho_0}{\rho_0 \Delta y_3^*} = \frac{M^4}{2\pi |\vec{x}^*| N} \frac{d^2}{dt^{*2}} \sum_{j=1}^{N} \left(\frac{\vec{x}^* \cdot \vec{x}_j^*}{|\vec{x}^*|} \right) \frac{\vec{x}^*}{|\vec{x}^*|} \cdot (\hat{e}_3 \times \vec{u}_j^*) \qquad (12)$$

where $M = \Gamma N/2\lambda c_0 = U/c_0$ is the mean flow Mach number, and $\Delta y_3^* = \Delta y_3/\lambda$. We may express Equation (12) in terms of polar coordinates $r^* = |\vec{x}^*|$ and $\theta = \tan^{-1} x_2^*/x_1^*$ in the plane x_3^* = constant as

$$\frac{\rho(r^*,\theta,t^*)-\rho_0}{\rho_0 \Delta y_3^*} = \frac{M^4}{2\pi r^*} [(\ddot{A}-\ddot{B})\cos 2\theta + \ddot{C} \sin 2\theta + \ddot{A} + \ddot{B}] \qquad (13)$$

where

$$A = -\frac{1}{2N} \sum_{j=1}^{N} x_{1,j}^* \, u_{2,j}^*$$

$$B = \frac{1}{2N} \sum_{j=1}^{N} x_{2,j}^* \, u_{1,j}^*$$

and

$$C = \frac{1}{2N} \sum_{j=1}^{N} (x_{1,j}^* \, u_{1,j}^* - x_{2,j}^* \, u_{2,j}^*)$$

The quantities A, B, and C are evaluated at time $t^*-M|\vec{x}^*|$.

3.2 CALCULATION OF SHEAR-LAYER HYDRODYNAMIC SOUND

Equation (13) provides a means for estimating the hydrodynamic sound generated by an unsteady vortical flow region approximated by a distribution of discrete point vortices. In this section we describe our application of Equation (13) to the sound emitted by a single spatial period of the shear layer.

The presence of third time derivatives of position in the expression poses significant difficulties. We found that numerical estimation of these derivatives with finite differences did not produce sufficiently accurate results without severe restrictions on the time-step size. We therefore chose to obtain these derivatives by analytically differentiating the equations of vortex motion, Equations (5) and (6). The resulting expressions directly relate $\ddot{x}_{1,j}$, $\ddot{x}_{2,j}$, $\dddot{x}_{1,j}$, and $\dddot{x}_{2,j}$ to $x_{1,j}$ and $x_{2,j}$ without truncation error (except that introduced in the calculation of $x_{1,j}$ and $x_{2,j}$). Note that all of the shear layer simulation results reported in this section were obtained with a sixth-order Milne predictor-corrector integration scheme applied to Equations (5) and (6).

Figures 3a and 3b display two stages in the evolution of the vortex system in the test case of motion with no external shear-layer disturbance. The layer is approximated by 126 vortices per unit length distributed initially in 18 equispaced columns, 7 vortices per column, and the calculation was performed with $\Delta t^*=0.00125$. This smaller number of vortices was used in acoustic model evaluation calculations to reduce the otherwise very large expense of performing computations with very small time steps. The figures suggest a great deal of energetic non-physical (numerical) vortex activity, and by $t^*=0.5$ (Figure 3b) significant numerical round-off error has accumulated. The regular pattern along the layer and the antisymmetry across the layer of vortex positions, which we expect in an exact calculation, is significantly eroded. We emphasize that this error is due to accumulated round-off in the calculation of the N-term sums in Equations (5) and (6), and not to truncation error in the integration scheme. Truncation error affects the position of the vortices in each row in an identical manner so that a regular vortex pattern would still result.

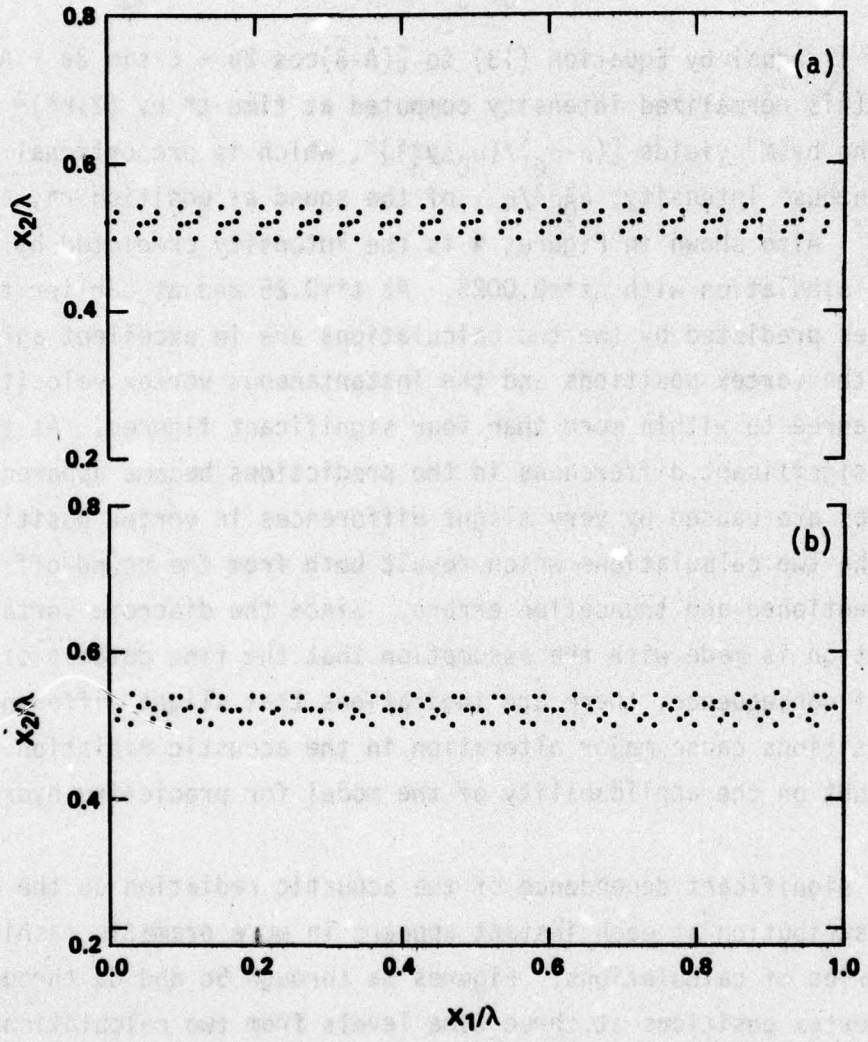

Figure 3. Position of vortices in shear layer with no applied disturbance: (a) t*=0.25; (b) t*=0.5. At t*=0.0, vortices are arranged in columns, seven per column.

The acoustic radiation as predicted from Equation (13) for the simulation described here is displayed in Figures 4a and 4b as a function of angle θ measured from the position x_1-direction. The radiation is presented in terms of a normalized "instantaneous" intensity which we define as

$$[(\frac{\rho-\rho_0}{\rho_0 \Delta y_3^*})(\frac{2\pi r^*}{M^4})]^2$$

and which is equal by Equation (13) to $[(\ddot{A}-\ddot{B})\cos 2\theta + \ddot{C} \sin 2\theta + \ddot{A} + \ddot{B}]^2$. Dividing this normalized intensity computed at time t* by $(2\pi r^*)^2$ and multiplying by M^8 yields $[(\rho-\rho_0)/(\rho_0 \Delta y_3^*)]^2$, which is proportional to the "instantaneous" intensity, $a_0^3\rho^2/\rho_0$, of the sound at position r*, θ at time t* + Mr*.[†] Also shown in Figures 4 is the intensity predicted by a second identical simulation with $\Delta t^*=0.0025$. At t*=0.25 and at earlier times the intensities predicted by the two calculations are in excellent agreement, and both the vortex positions and the instantaneous vortex velocities were found to agree to within more than four significant figures. At t*=0.5, however, significant differences in the predictions became apparent. These differences are caused by very slight differences in vortex position between the two calculations which result both from the round-off error already mentioned and truncation errors. Since the discrete vortex approximation is made with the assumption that the fine details of the flow are not of consequence, there are indications that slight differences in vortex positions cause major alteration in the acoustic radiation. This throws doubt on the applicability of the model for predicting hydrodynamic noise.

The significant dependence of the acoustic radiation on the detailed vortex distribution at each instant appears in more dramatic fashion in a second series of calculations. Figures 5a through 5c and 6a through 6c display vortex positions at three time levels from two calculations of the layer evolution resulting from a single-wave disturbance. In the simulation depicted in Figures 5a through 5c 126 vortices are "stacked" in

---

[†] The intensity of sound, I, is defined as the average rate at which energy is transported across a unit area normal to the propagation direction, so that $I = c_0\langle\rho^2\rangle/\rho_0$ where $\langle\ \rangle$ denotes time average.

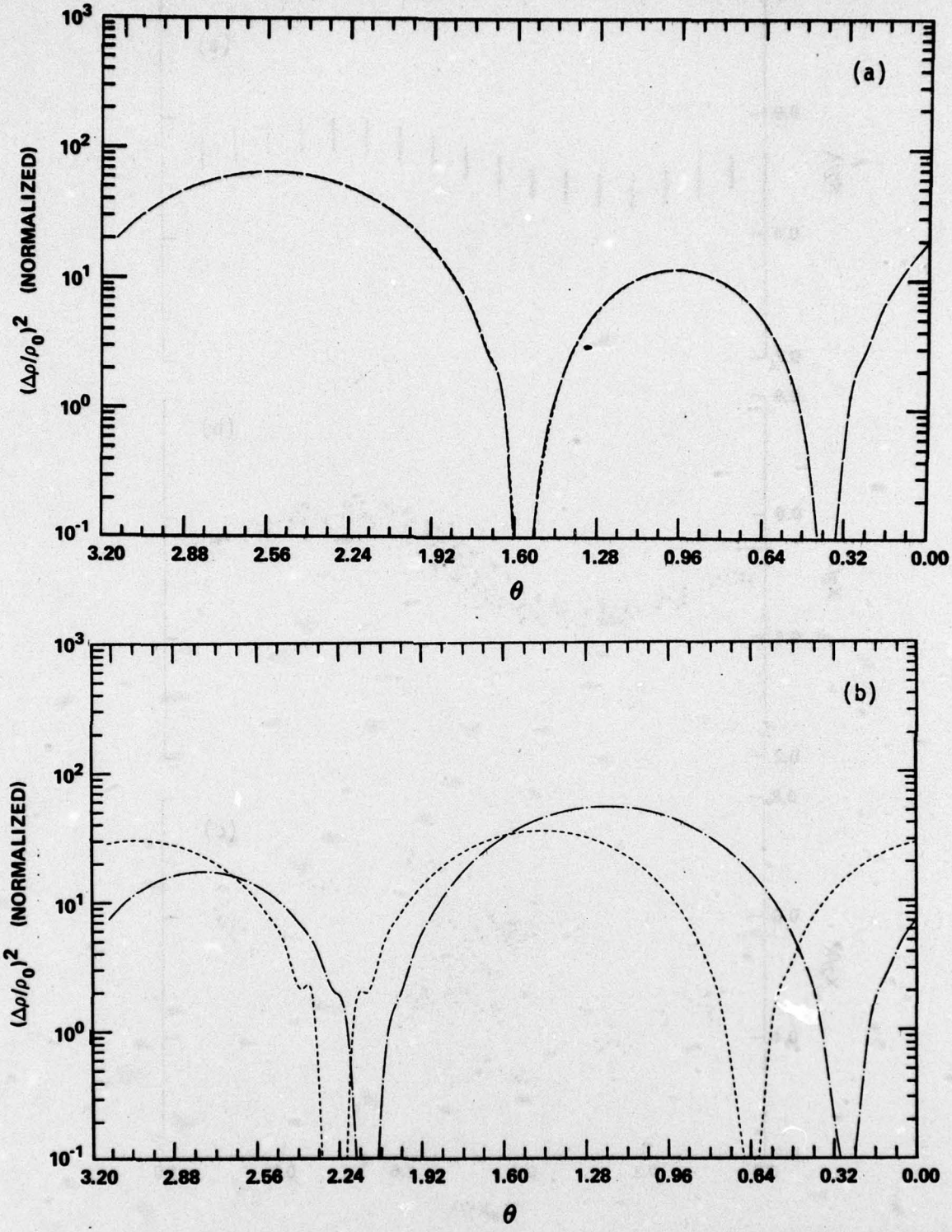

Figure 4. Effect of time-step size on acoustic radiation from a shear layer with no applied disturbance (Fig. 3): (a) $t^*=0.25$; (b) $t^*=0.5$. Dashed lines, $\Delta t^*=0.0025$; chain-dotted lines, $\Delta t^*=0.00125$.

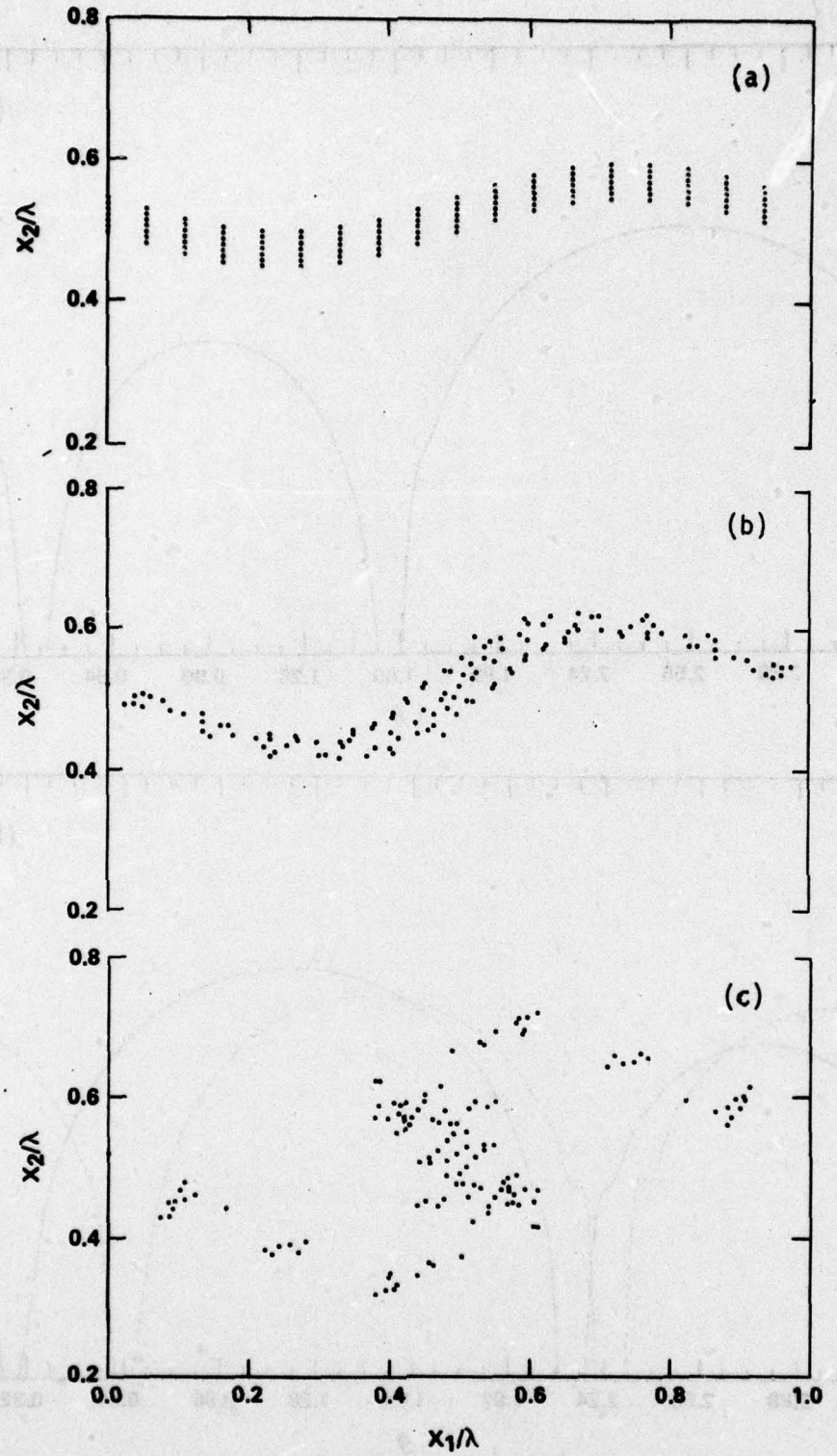

Figure 5. Position of vortices in shear layer resulting from a single-wave disturbance: (a) t*=0.0; (b) t*=0.25; (c) t*=0.5. At t*=0.0, vortices are arranged in columns, seven per column.

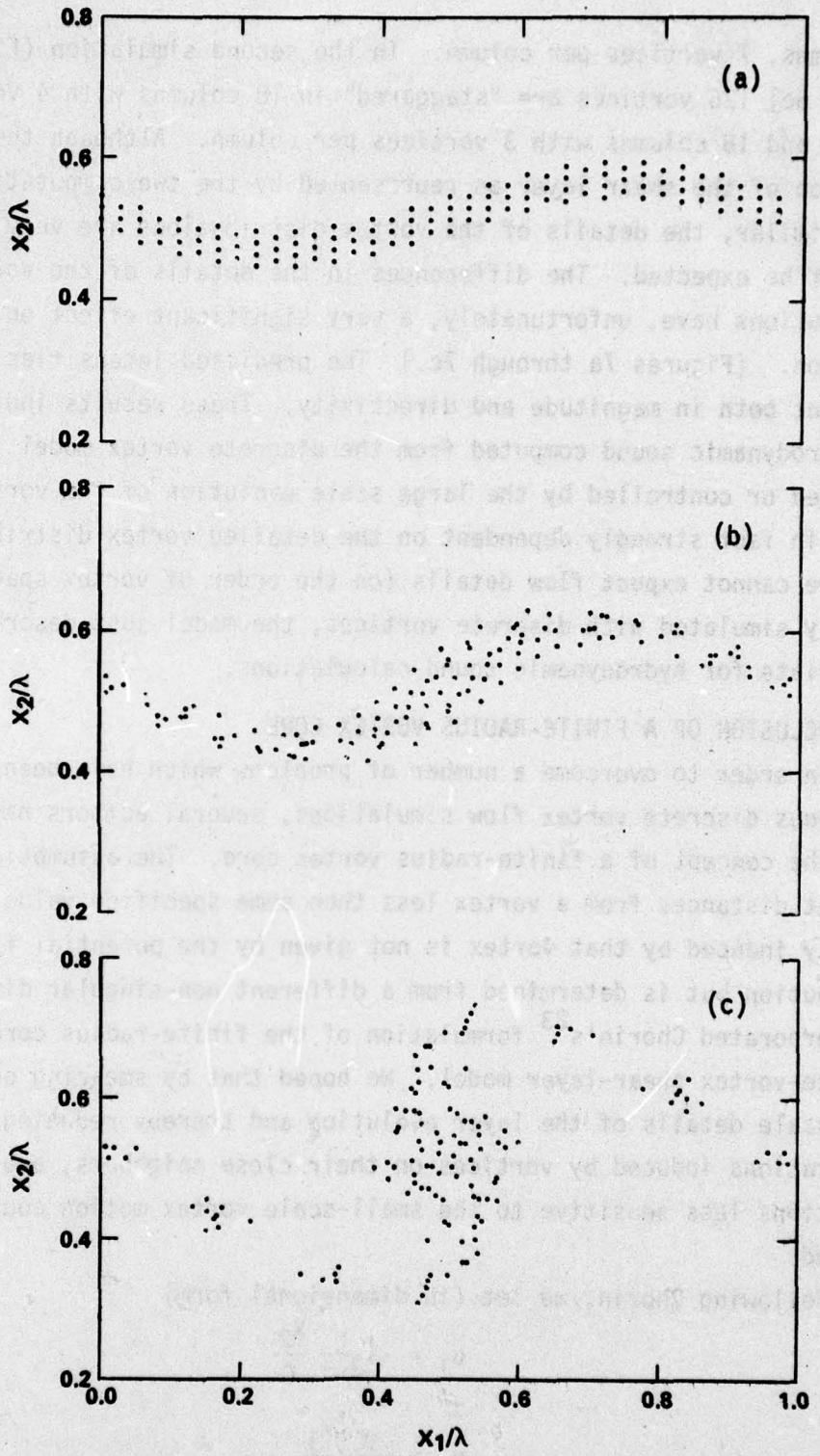

Figure 6. Position of vortices in shear layer resulting from a single-wave disturbance: (a) t*=0.0; (b) t*=0.25; (c) t*=0.5. At t*=0.0, vortices are arranged in columns, 4 vortices per column and 3 vortices per column.

18 columns, 7 vortices per column. In the second simulation (Figs. 6a through 6c) 126 vortices are "staggered" in 18 columns with 4 vortices per column, and 18 columns with 3 vortices per column. Although the over-all evolution of the shear layer as represented by the two computations is quite similar, the details of the vortex distributions are very different as might be expected. The differences in the details of the vortex distributions have, unfortunately, a very significant effect on the acoustic radiation. (Figures 7a through 7c.) The predicted intensities are quite different both in magnitude and directivity. These results indicate that the hydrodynamic sound computed from the discrete vortex model is not dominated or controlled by the large scale evolution of the vortex system, but is in fact strongly dependent on the detailed vortex distribution. Since we cannot expect flow details (on the order of vortex spacings) to be properly simulated with discrete vortices, the model just described is not appropriate for hydrodynamic sound calculations.

3.3 INCLUSION OF A FINITE-RADIUS VORTEX CORE

In order to overcome a number of problems which have been encountered in various discrete vortex flow simulations, several authors have introduced the concept of a finite-radius vortex core. The assumption is made that, at distances from a vortex less than some specified value, the velocity induced by that vortex is not given by the potential flow r^{-1} distribution but is determined from a different non-singular distribution. We incorporated Chorin's[23] formulation of the finite-radius core into the discrete-vortex shear-layer model. We hoped that by smearing out the small-scale details of the layer evolution and thereby reducing the large accelerations induced by vortices on their close neighbors, acoustic predictions less sensitive to the small-scale vortex motion could be obtained.

Following Chorin, we let (in dimensional form)

$$u_1 = -\frac{\Gamma}{2\pi\sigma}\frac{x_2}{r}$$

and

$$u_2 = \frac{\Gamma}{2\pi\sigma}\frac{x_1}{r}$$

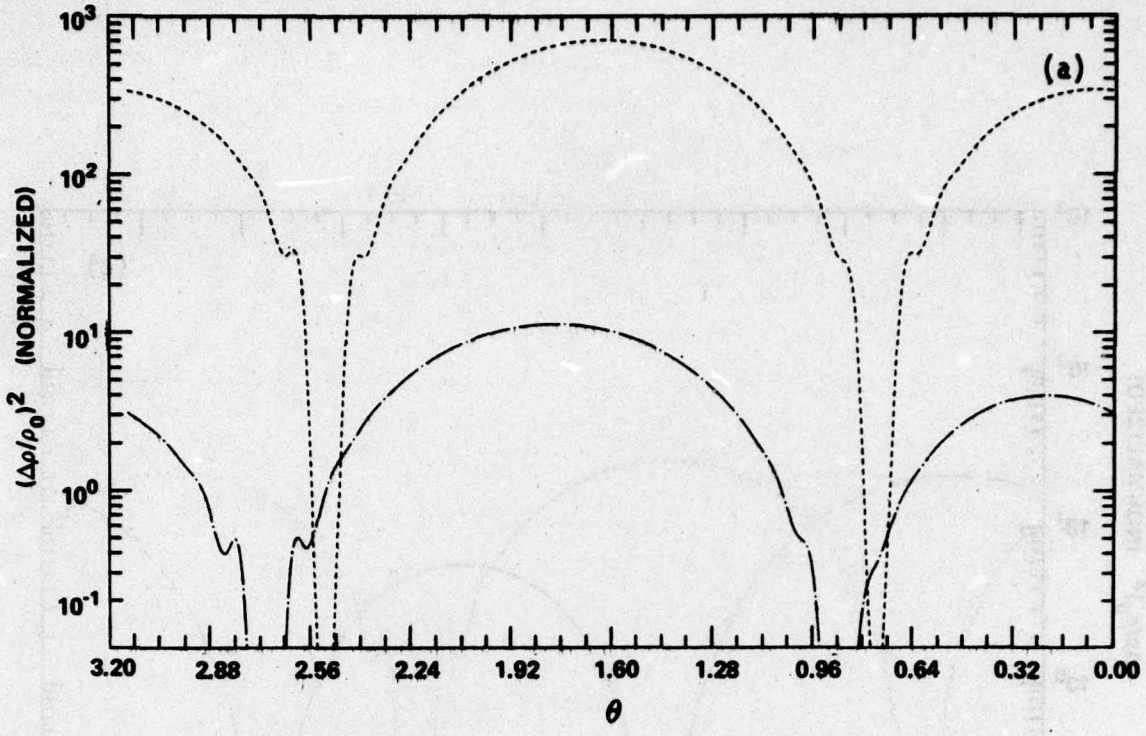

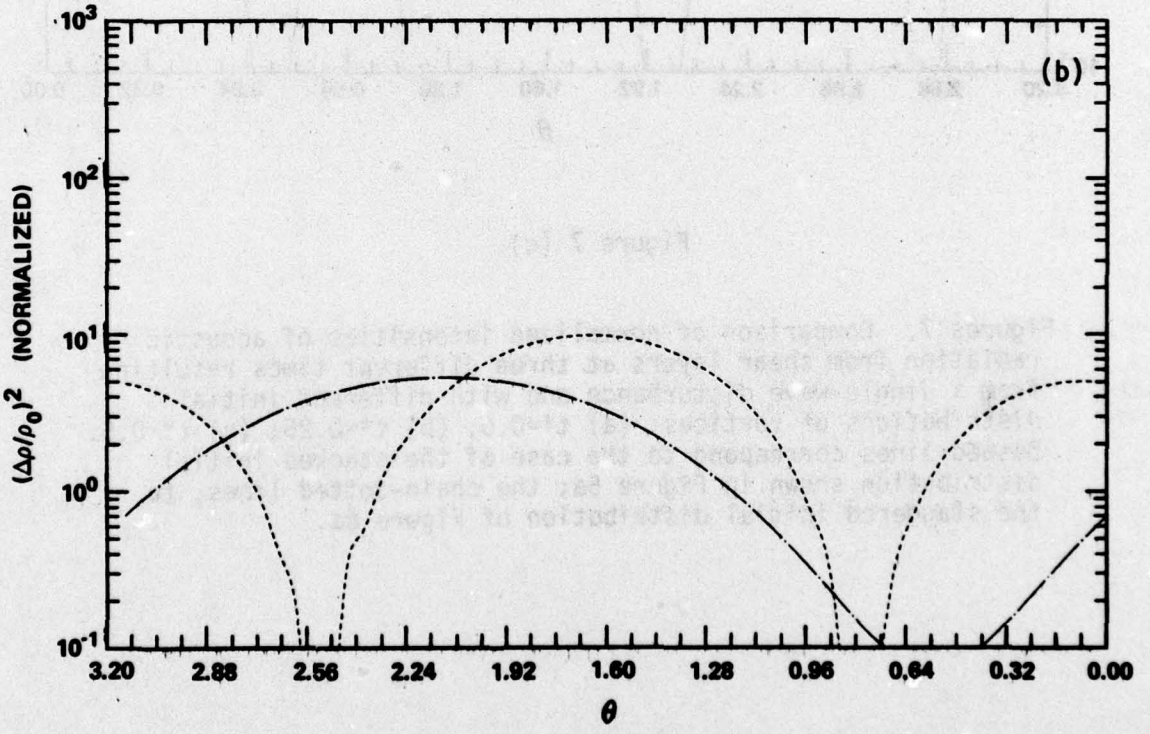

Figures 7 (a,b). For legend see next page.

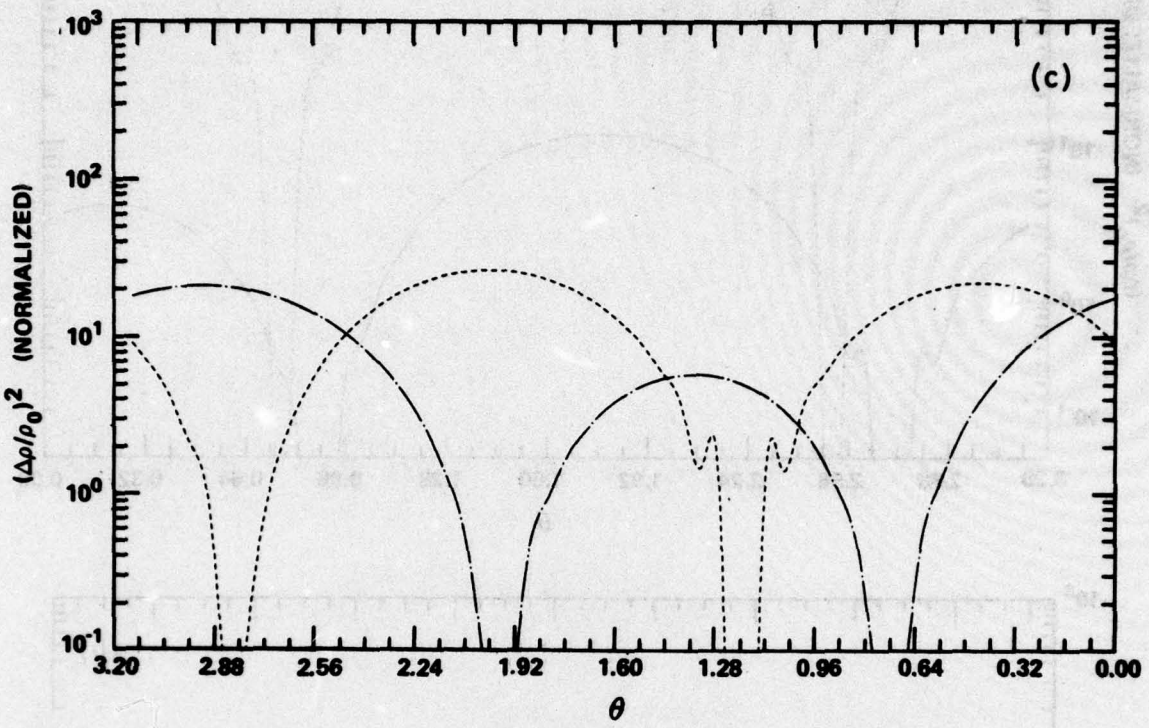

Figure 7 (c).

Figures 7. Comparison of normalized intensities of acoustic radiation from shear layers at three different times resulting from a single-wave disturbance and with different initial distributions of vortices: (a) t*=0.0; (b) t*=0.25; (c) t*=0.5. Dashed lines correspond to the case of the stacked initial distribution shown in Figure 5a; the chain-dotted lines, to the staggered initial distribution of Figure 6a.

with $r = \sqrt{x^2+y^2}$, denote the components of the velocity at (x_1,x_2) induced by a vortex at the origin. These expressions are applied at $r \leq \sigma$ where σ is the core radius; for $r > \sigma$ the r^{-1} profile is applied. The combined velocity expression thus exhibits the potential flow distribution outside the core and finite values of u_1 and u_2 inside the core.

A number of computations were performed with several values of the core radius σ. These calculations show that, even with σ as large as one-third of the initial shear-layer thickness, the large-scale evolution of the layer is not appreciably affected. The small-scale behavior of the layer is, however, drastically affected and, in general, the intensity is significantly lowered. Figures 8a through 8c compare the predicted intensities (with a core radius of one-third the initial shear layer thickness) for a computation beginning with the "stacked" vortex distribution shown in Figure 5a and a computation beginning with the "staggered" distribution shown in Figure 6a. The intensities predicted by both the "stacked" and "staggered" computations are a good deal lower than those predicted without the finite-radius core (Figures 7b and 7c). This might be expected since the accelerations and time rates of acceleration change of closely spaced vortices are substantially reduced and these quantities are significant in the acoustic prediction (see Equation (13)). The intensities at $t^*=0.5$ predicted from the "stacked" and "staggered" computations are encouragingly similar but by $t^*=0.75$ they are quite different so that there is, unfortunately, no indication that the critical influence of the initial vortex distributions on the acoustic radiation lessens as the vortex system evolves.

4. SUMMARY AND CONCLUSIONS

We have shown that a discrete vortex model of the two-dimensional shear layer effectively models the large scale evolution and behavior of the layer resulting from the application of an imposed disturbance. An identical conclusion was reached by Acton.[18] The over-all behavior of the layer is in qualitative agreement with the experimental observations of Winant and

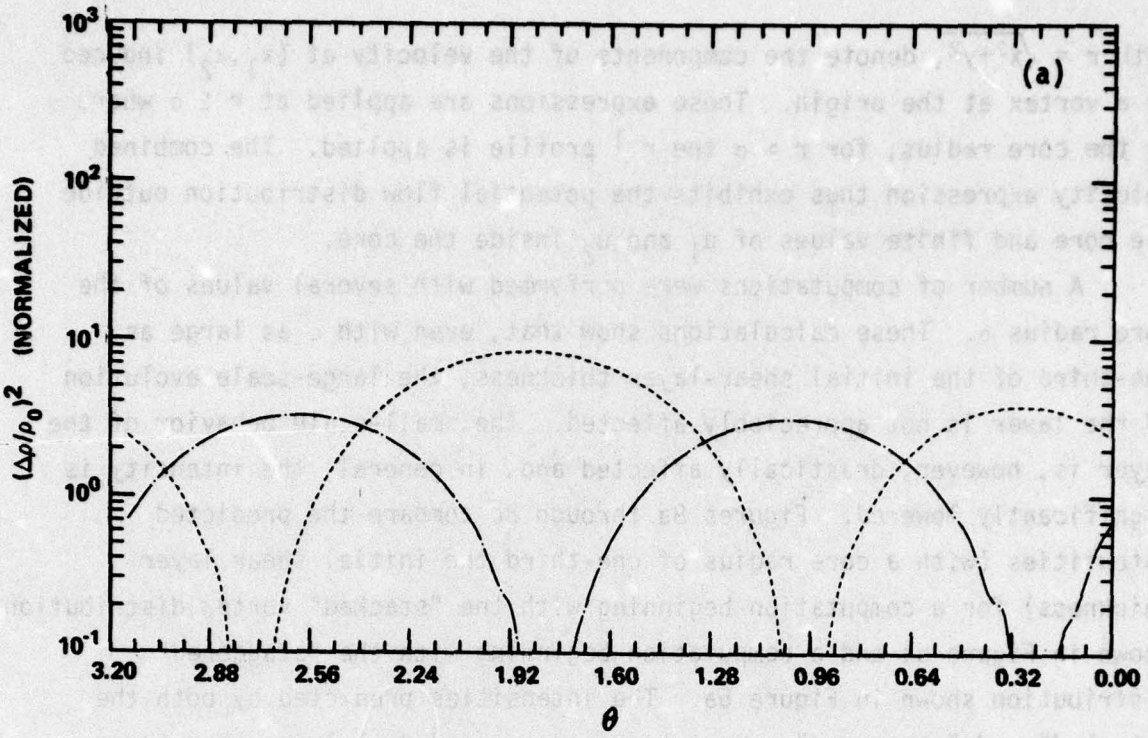

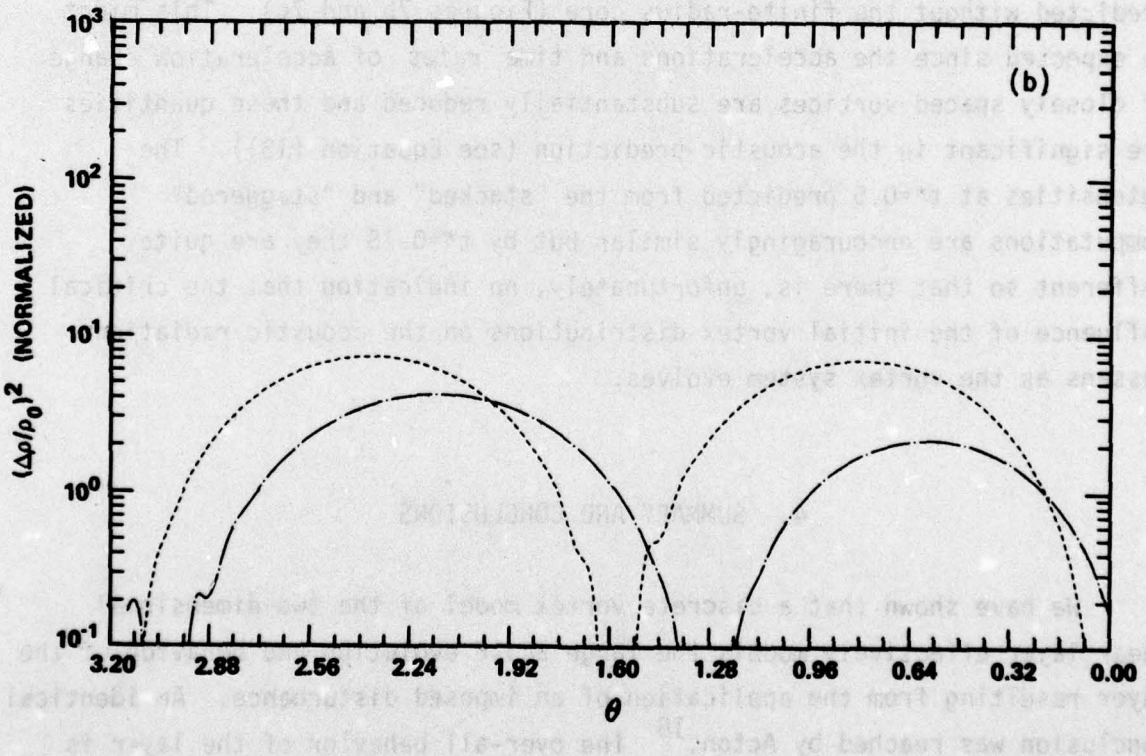

Figures 8 (a,b). For legend see next page.

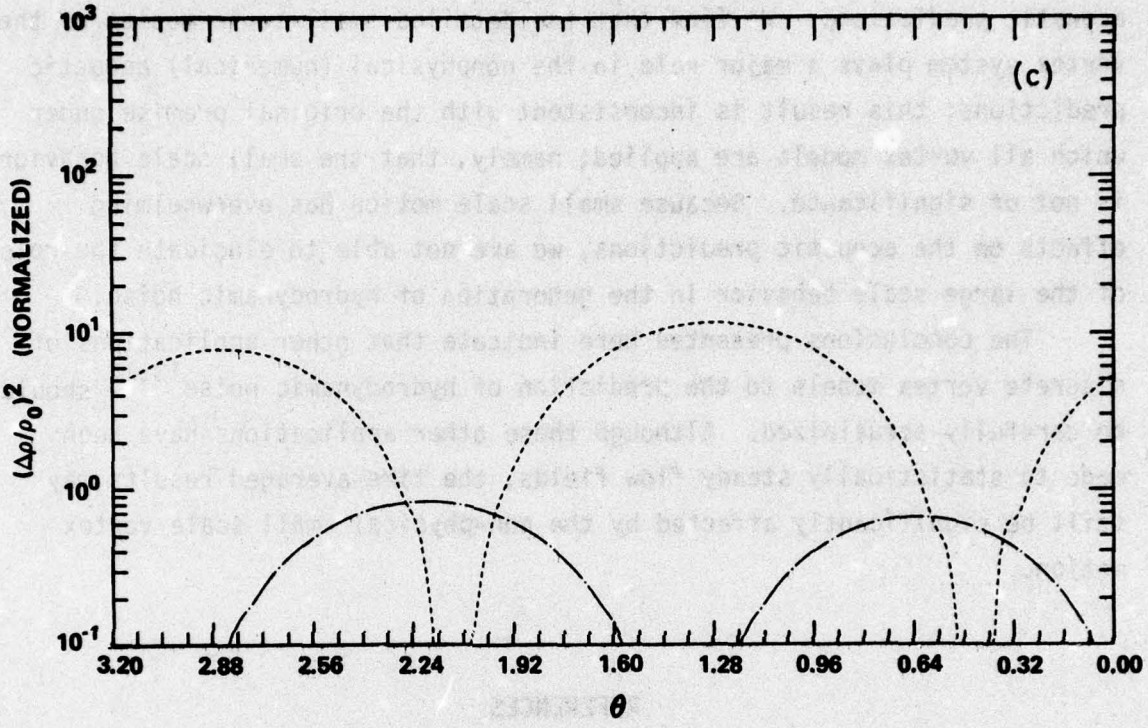

Figure 8 (c).

Figures 8. Comparison of normalized intensities of acoustic radiation from shear layers at three different times (with Chorin's finite-radius core) resulting from a single-wave disturbance and with different initial distributions of vortices: (a) $t^*=0.25$; (b) $t^*=0.5$; (c) $t^*=0.75$. Dashed lines correspond to the case of the stacked initial distribution shown in Figure 5a; the chain-dotted lines, to the staggered initial distribution of Figure 6a.

Browand.[4] However, although we are aware of no directly relevant data with which to compare the model estimates of the hydrodynamic sound generated in the layer, our investigation has led us to conclude that the vortex model is not an appropriate representation of the shear layer for acoustic predictions. We find that the detailed small-scale motion of the vortex system plays a major role in the nonphysical (numerical) acoustic predictions; this result is inconsistent with the original premise under which all vortex models are applied; namely, that the small scale behavior is not of significance. Because small scale motion has overwhelming effects on the acoustic predictions, we are not able to elucidate the role of the large scale behavior in the generation of hydrodynamic noise.

The conclusions presented here indicate that other applications of discrete vortex models to the prediction of hydrodynamic noise[13,14] should be carefully scrutinized. Although these other applications have been made to statistically steady flow fields, the time-averaged results may still be significantly affected by the non-physical small-scale vortex motion.

REFERENCES

1. Roshko, A., "Structure of Turbulent Shear Flows: A New Look," AIAA Journal, Vol. 14, p. 1349 (1976).
2. Townsend, A.A., The Structure of Turbulent Shear Flow, Cambridge University Press, 1956.
3. Brown, G.L. and Roshko, A., "On density effects and large structure in turbulent mixing layers," J. Fluid Mech., Vol. 64, p. 775 (1974).
4. Winant, C.D. and Browand, F.K., "Vortex pairing: the mechanism of turbulent mixing layer growth at moderate Reynolds number," J. Fluid Mech., Vol. 63, p. 237 (1974).
5. Kim, H.T., Kline, S.J. and Reynolds, W.C., "The production of turbulence near a smooth wall in a turbulent boundary layer," J. Fluid Mech., Vol. 50, p. 133 (1971).

6. Kline, S.J., Reynolds, W.C., Schrab, F.A. and Rundstadler, P.W., "Structure of turbulent boundary layers," J. Fluid Mech., Vol. 30, p. 741 (1967).
7. Offen, G.R. and Kline, S.J., "Combined dye-streak and hydrogen-bubble visual observations of a turbulent boundary layer," J. Fluid Mech., Vol. 62, p. 223 (1974).
8. Crow, S.C. and Champagne, F.H., "Orderly structure in jet turbulence," J. Fluid Mech., Vol 48, p. 547 (1971).
9. Moore, C.J., "The role of shear-layer instability waves in jet exhaust noise," J. Fluid Mech., Vol. 80, p. 321 (1977).
10. Lau, J.C. and Fisher, M.J., "The vortex-street structure of 'turbulent' jets, part 1," J. Fluid Mech., Vol. 67, p. 229 (1975).
11. Crow, S.C., "Acoustic Gain of a Turbulent Jet," Meeting Div. Fluid Dyn. Am. Phys. Soc., Univ. Colorado, Paper IEG (1972).
12. Crighton, D.G., "AIAA 3rd Aeroacoustics Conference," DTNSRDC Ship Acoustics Department TM-06-1900 (1976).
13. Davies, P.O.A.L., Hardin, J.C., Edwards, A.V.J. and Mason, J.P., "A Potential Flow Model for Calculation of Jet Noise," Progress in Astronautics and Aeronautics, Vol. 43 (1976).
14. Hardin, J.C. and Mason, J.P., "A Vortex Model of Cavity Flow," Third AIAA Aeroacoustics Conference, Palo Alto, CA (1976).
15. Powell, A., "Theory of Vortex Sound," J. Acoust. Soc. Am., Vol 36, p. 177 (1964).
16. Metcalfe, R.W. and Orszag, S.A., "Numerical Simulation of Turbulent Jet Noise. I," Rept. 53, Flow Research, Inc., Kent, WA (1974).
17. Metcalfe, R.W., private communication (1977).
18. Acton, E., "The modelling of large eddies in a two-dimensional shear layer," J. Fluid Mech., Vol. 76, p. 561 (1976).
19. Ashurst, W.T., "Numerical Simulation of Turbulent Mixing Layers via Vortex Dynamics," Report SAND77-8613, Sandia Laboratories, Livermore, CA (1977).
20. Browand, F.K. and Weidman, P.D., "Large scales in the developing mixing layer," J. Fluid Mech., Vol. 76, p. 127 (1976).

21. Lighthill, M.J., "On sound generated aerodynamically. I. General Theory," Proc. Roy. Soc. Series A, Vol. 211, p. 564 (1952).

22. Howe, M.S., "Contributions to the theory of aerodynamic sound, with application to excess jet noise and the theory of the flute," J. Fluid Mech., Vol. 71, p. 625 (1975).

23. Chorin, A.J., "Numerical Study of Slightly Viscous Flow," Report No. FM-72-4, Department of Mechanical Engineering, University of California, Berkeley (1972).

DISTRIBUTION LIST

Copies:

CHONR

1 102
1 430/R.J. Lundegard
1 430B/M. Cooper
1 432/L.D. Bram
1 434/T.C. Varley
1 436/B.J. MacDonald
1 438/R.D. Cooper

NAVPGSCHOL

1 T. Sarpkaya
1 Math Dept
1 Library

NSWC/Dahlgren

1 A.V. Hershey
1 Library

NAVSEA

1 03C
1 0311
1 033
1 09G32
1 RAAD-3
1 RAAD-22
1 SP-26

1 NAVSHIPYD BREM/Lib
1 NAVSHIPYD CHASN/Lib
1 NAVSHIPYD MARE/Lib
1 NAVSHIPYD NORVA/Lib
1 NAVSHIPYD PEARL/Lib
1 NAVSHIPYD PHILA/Lib
1 NAVSHIPYD PTSMH/Lib

NAVSEC

1 6113B6/P.A. Gale
1 6114/R.S. Johnson

12 DDC

1 BUSTAND/Lib

1 NASA HQS/Lib

NASA AMES RES CEN

1 E.D. Martin
1 R.W. MacCormack
1 Library

NASA LANGLEY RES CEN

1 J.C. Hardin
1 Library

NASA LEWIS RES CEN

1 Library

NASA MARSHALL SFC

1 Library

1 U BRISTOL/R.R. Clements

2 U CALIF
S. Berger
A. Chorin

1 CORNELL U/K.E. Torrance

1 Dynamics Technology, Inc./D.R.S. Ko

1 Flow Research, Inc./J. Riley

1 Rand Corp/Lun-Shin Yao

10 Sci Applications, Inc/W.J. Grabowski

DTNSRDC Dist:

1 00
1 01
1 1800
1 1802.2
1 1805
1 1809.3
1 182
1 184
1 1843 J.Schot
10 1843 J.Telste
1 1844 S.Dhir
1 185
1 187
1 189
1 1900 M. Sevik
1 5211
1 522
1 522.2

DTNSRDC ISSUES THREE TYPES OF REPORTS

1. DTNSRDC REPORTS, A FORMAL SERIES, CONTAIN INFORMATION OF PERMANENT TECHNICAL VALUE. THEY CARRY A CONSECUTIVE NUMERICAL IDENTIFICATION REGARDLESS OF THEIR CLASSIFICATION OR THE ORIGINATING DEPARTMENT.

2. DEPARTMENTAL REPORTS, A SEMIFORMAL SERIES, CONTAIN INFORMATION OF A PRELIMINARY, TEMPORARY, OR PROPRIETARY NATURE OR OF LIMITED INTEREST OR SIGNIFICANCE. THEY CARRY A DEPARTMENTAL ALPHANUMERICAL IDENTIFICATION.

3. TECHNICAL MEMORANDA, AN INFORMAL SERIES, CONTAIN TECHNICAL DOCUMENTATION OF LIMITED USE AND INTEREST. THEY ARE PRIMARILY WORKING PAPERS INTENDED FOR INTERNAL USE. THEY CARRY AN IDENTIFYING NUMBER WHICH INDICATES THEIR TYPE AND THE NUMERICAL CODE OF THE ORIGINATING DEPARTMENT. ANY DISTRIBUTION OUTSIDE DTNSRDC MUST BE APPROVED BY THE HEAD OF THE ORIGINATING DEPARTMENT ON A CASE-BY-CASE BASIS.